EPJ Web of Conferences **3**, 01005 (2010)
DOI:10.1051/epjconf/20100301005


# The Weak Structure of the Nucleon

D. Gazit[1,2,a]

[1] Institute for Nuclear Theory, University of Washington, Seattle, WA 98195-1550, USA.
[2] Racah Institute of Physics, Hebrew University of Jerusalem, Jerusalem 91904, Israel.

**Abstract.** The weak structure of the nucleon is the non-perturbative response of the nucleon to a weak-interacting probe. Here, I review the existing experimental data at low energy. In particular, the role of few-body nuclear reactions in constraining the weak response of the nucleon, in vacuum and in nuclear medium, is discussed.

## 1 Introduction

The nucleon is the basic component of the nucleus. The nucleon itself is not a point particle, as its structure, i.e., its response to an external probe, varies with the momentum of this probe. In fact, the character of the probe affects the deduced structure as well. For example, the baryon radius of the nucleon is about 0.5 fm, the axial radius is about 0.65 fm, and the charge radius about 0.85 fm. As the structure is determined by the fundamental theory, quantum chromo-dynamics (QCD), it is used to constrain the theory. The weak structure at low energies, which is the subject of this contribution, determines weak reaction rates with nuclei, which are the motor of astrophysical phenomena, such as solar fusion, core collapse supernovae and the nucleosynthesis within. In addition, these reactions are used to study nuclear structure and dynamics. High accuracy theoretical and experimental understanding of the nucleon response is a key ingredient needed to accomplish these tasks.

However, the non-perturbative character of QCD at low energies makes a theoretical calculation of this response terribly challenging, a challenge that is only partially met today by means of large scale lattice-QCD calculations, which have a $\sim 5\%$ accuracy, as well as systematic problems originated in the basic assumptions of the method. Moreover, this property of QCD entails that even though the probe can be treated perturbatively, the nucleon itself has to be treated non-perturbatively. As a result, one usually resorts to an experimental study of this response. In the case of the response of a nucleon to a weak probe, even the experimental measurement of the response becomes hard, as the cross-sections are very small.

The purpose of this contribution is to advocate that few-body nuclear physics has a central role in solving this problem. Few-body nuclear physics is at the dawn of a precision era, due to two main reasons. The first is the evolution of mathematical methods developed to solve the quantum mechanical nuclear problem from its nucleonic degrees of freedom. Prominent examples are the Green's function monte carlo, no-core shell model, expansions in hyperspherical harmonics, and direct solutions of the Fadeev-Yakubovsky equations [1–5]. Alongside these methods, the growing available computational power has allowed *ab*-initio calculations of the structure of $A \leq 16$ nuclei, as well as inelastic cross-sections of $A \leq 7$, from the nucleonic degrees of freedom.

The second ingredient, developed in the last two decades, is chiral perturbation theory ($\chi$PT) – an effective theory of QCD at low energies, enabling a construction of a nuclear Lagrangian that is consistent with QCD. The combination of these two ingredients allows essentially parameter free calculations of weak nuclear reactions, with sub-percentage accuracy. This allows, on the one hand, an extraction of the properties of the nucleon from nuclear reactions, and on the other hand facilitates a research of the aforementioned tasks.

The paper is built in the following way. In the next section, I present the theoretical tools needed for the calculation of weak reactions, including a description of the weak structure of the nucleon. I then outline in Sec. 2 an approach to calculate weak interaction of probes with nuclei, based on $\chi$PT. The last three sections are dedicated to describe calculations of three specific reactions, intended to study the weak structure of the nucleon, its evolution inside nuclei, and implications of weak reactions on our understanding of nuclear structure.

## 2 Weak interaction processes in the standard model

The weak coupling constant $G = 1.166 \times 10^{-11}\,\mathrm{MeV}^{-2}$ provides a small parameter in the interaction of leptons and hadronic matter. As a result, the scattering processes is well approximated by one gauge boson exchange. A lepton of momentum $k_i^\mu$ interacts with a nucleus of initial momentum $P_i^\mu$, via the exchange of a heavy boson with momentum $q^\mu = (\omega, \mathbf{q})$, resulting in an outgoing lepton with

[a] e-mail: doron.gazit@mail.huji.ac.il

momentum $k_f^\mu$, and nuclear fragments with momentum $P_f^\mu$. Energy momentum conservation implies: $q^\mu = k_i^\mu - k_f^\mu = P_f^\mu - P_i^\mu$.

Thus, the general form of the transition matrix element for both charge changing and neutral reaction is:

$$T_{fi} = (\text{lepton current})^\mu \cdot \frac{g_{\mu\nu} + \frac{q_\mu q_\nu}{q^2}}{q^2 + M_B^2} \cdot (\text{hadronic current})^\nu . \quad (1)$$

For low energy reactions with respect to the boson mass – $M_{Z^0} \approx 92\,\text{GeV}$ (for neutral reactions) or $M_{W^\pm} \approx 80\,\text{GeV}$ (for charge changing reactions) – the momentum dependent terms are negligible. The boson propagator reduces in this limit to $g_{\mu\nu}/M_B^2$, and acts as an effective point interaction. This effective vertex leads to the famous current–current Hamiltonian density: $\mathcal{H}_W \sim j^\mu \mathcal{J}_\mu$ ($j^\mu$ is the lepton current, and $\mathcal{J}_\mu$ is the nuclear current). The leptons are point Dirac fermions, and thus their current results in kinematical factors to the reaction rate. The hadronic currents are more complicated. Here, we concentrate in the case where the pertinent quarks are up-quark and down-quark, assuming SU(2) symmetry, and a decoupling of the heavier quarks. The standard model predicts that the nuclear, or hadronic, currents, can be written as,

$$\mathcal{J}_\mu^{(0)} = (1 - 2 \cdot \sin^2\theta_W)\mathcal{V}_\mu^0 + \mathcal{A}_\mu^0 - 2 \cdot \sin^2\theta_W \mathcal{I}_\mu \quad (2)$$
$$\mathcal{J}_\mu^{(\pm)} = \mathcal{V}_\mu^\pm + \mathcal{A}_\mu^\pm$$

Where $\theta_W$ is the mixing of the weak and electro-magnetic forces, affecting only the neutral current. In addition:

- $\mathcal{V}_\mu^a = \bar{q}\frac{\tau^a}{2}\gamma_\mu q$ is the isovector current of polar symmetry ($q$ is the quark field).
- $\mathcal{A}_\mu^a = \bar{q}\frac{\tau^a}{2}\gamma_5\gamma_\mu q$ is the isovector current of axial symmetry.
- $\mathcal{I}_\mu^a = \frac{1}{2}\bar{q}\gamma_\mu q$ is the isoscalar current of vector symmetry.

Since we restrict ourselves to the SU(2), $\tau$ are Pauli matrices. Had we included the strange quark as well, one would replace these by the Gell-Mann SU(3) matrices. The implications of including the strange quark, and its affect on nucleonic structure function is studied via the neutral current, as the strange quark leads contributes to the isoscalar current, a subject which will not be dealt in the current contribution [6]. In addition, since most experimental data comes from charge-changing reactions, we will focus in this case.

In nuclear reactions, the quarks are bound, and one has to consider the matrix element of the different currents taken between the nuclear states. This matrix element is the internal weak structure of the nucleus, probed to a resolution that corresponds to the energy of the lepton. When taken between nucleonic states, this matrix elements corresponds to the weak structure of the nucleon.

### 2.1 The weak structure of the nucleon

Though a calculation of the response of the nucleon to a weak probe involves a solution of QCD at low-energies, the symmetries of the theory, as well as the fact that the nucleon is a spin 1/2 entity, help us in phenomenologically constraining the structure of the nucleon. Using just the Lorentz symmetry, one can write the nucleonic currents as a combination of the only vector in the system, namely the momentum transfer, and the Dirac matrices:

$$\left\langle N(p')|\mathcal{V}_\mu^a|N'(p)\right\rangle = \quad (3)$$
$$\bar{u}(p')\left\{F_V(q^2)\gamma_\mu + \frac{iF_M(q^2)}{2M_N}\sigma_{\mu\nu}q^\nu + F_S(q^2)q_\mu\right\}\frac{\tau^a}{2}u(p)$$
$$\left\langle N(p')|\mathcal{A}_\mu^a|N'(p)\right\rangle = \quad (4)$$
$$-\bar{u}(p')\left\{G_A(q^2)\gamma_\mu + \frac{iG_P(q^2)}{2M_N}q_\mu + G_T(q^2)\sigma_{\mu\nu}q^\nu\right\}\gamma_5\frac{\tau^a}{2}u(p).$$

Adding the discrete C, P, and T symmetries, constrains the weak form factors $F_V$, $F_M$, $F_S$, $G_A$, $G_P$, and $G_T$ to be real. In the quark level, as dictated by the standard model, $F_V(q^2) = G_A(q^2) = 1$, whereas $F_S = F_M = G_P = G_T = 0$. The last four form factors are induced by the strong interaction. Thus, they are determined by the symmetries and properties of this interaction.

In particular, the quark currents have a specific behavior under G-parity, i.e., the combination of charge symmetry and rotation in isospin space $\hat{C}\exp(i\pi\hat{T}_2)$ [7]. Had the strong interaction been invariant under G-parity as well, the induced pseudo-tensor and induced scalar form factors would vanish as they precede operators that have opposite behavior under G-parity. These two form factors are called second class currents due to this reason, and there is no experimental evidence for their existence. Indeed, the strong interaction is charge-independent. Isospin symmetry, however, is only approximate, due to finite mass difference between the up and down masses. We thus expect that the second class currents will not vanish exactly, but will be highly suppressed by a factor of $\frac{m_d - m_u}{2M_N}$. The experimental search for second class currents is a very active field, as, depending on the size of the couplings, it can be used to constrain beyond the standard model scalar and pseudo-tensor couplings [8].

### 2.2 Vector structure of the nucleon

From Eq. 3, one easily finds that at zero momentum transfer $1 = \left\langle p|\mathcal{V}_0^+|n\right\rangle = F_V(0)$ (the first equality is due to normalization of the quark composed wave functions, while the second is from the normalization of nucleonic wave functions). Thus, $F_V$, the vector form factor, is not renormalized when going from the quark level to the nucleonic level. The same holds for the nucleus level. The fact that correlations do not affect the single particle matrix element, has led Gerstein and Zeldovich, and independently Feynman and Gell-Mann, to the Conservation of Vector Current (CVC) hypothesis [9].

According to this hypothesis: (i) the charge changing ($a = \pm$) components of the weak vector current and the isovector part of the electromagnetic current are three components of the same iso-vector, (ii) each of the components is conserved.

In retrospect, in view of the standard model, the first part is indeed correct, and $\left(\mathcal{V}^{\gamma}, \frac{\mathcal{V}^{\pm}}{\cos\theta_C}\right)$ is an isovector ($\theta_C$ is the Cabbibo mixing angle). The second part is not exact, due to isospin breaking. However, the conservation of the weak vector current is an excellent approximation, that has no experimental deviations, and predicted theoretically to be exact to the $10^{-4}$ level [10].

The ramifications of CVC are immense:

- The vector form factor $F_V$ and the weak magnetic form factor $F_M$ are equal to the electro-magnetic electric and magnetic form factors, where they are constrained to great accuracy.
- The induced scalar form factor vanishes.
- One can use the Siegert theorem for weak reactions.

A most successful experimental way to test CVC is by observing superallowed $0^+ \to 0^+$ $\beta$ decays. In such cases, only the vector current contributes. CVC predicts that up to radiative corrections and a small nuclear correction $\delta_C$, the "comparative" half-life (a term that will be described exactly later) of all these decays should be equal. Towner and Hardy [11] used this to constrain the induced scalar form factor to $m_e F_s/F_V = -0.0011(13)$, and the unitarity of the CKM matrix to $6 \times 10^{-4}$ level. However, their calculation of the nuclear corrections was recently challenged by Miller and Schwenk [12] due to inconsistencies in the isospin algebra. A different calculation of this is needed. In the field of few-body nuclear physics it seems that the only superallowed decay which is at reach is the decay of $^{10}$C to the excited state of $^{10}$B. A previous calculation [13] using a no-core shell model approach up to $N_{max} = 8$ and the CD-Bonn potential has shown no sign of convergence, and even at the largest model space exhausted only $10-20\%$ of the correction. Thus, this problem remains as a challenge to few-body nuclear physicists, due to its importance for the unitarity of the CKM matrix and as these results are quoted in the Particle data group compilations [14].

### 2.3 Axial structure of the nucleon

Similarly to the vector current, there is no evidence to second class currents also in the axial currents. Contrary to the vector current, the axial current is neither conserved, nor close to that. For this reason, the axial constant is renormalized from its value at the nucleon level to $g_A = G_A(0) = 1.2695(29)$ [14]. This value is extracted from the half life of a neutron, with the assumption of $F_V(0) = 1$. This value is recovered by lattice QCD calculations to about 7%. A recent calculation using AdS/QCD correspondence has given $g_A \approx 1.3$, which shows some of the promise in calculating nuclear couplings in this model [15].

At finite, albeit small, momentum transfer, one can parameterize the deviation from this value either by a dipole form or by defining an axial radius, which is determined by neutrino scattering and pion electroproduction [16].

Contrary to the accuracy in the measurement of $G_A$ at low energy, the induced pseudo-scalar is rather poorly known experimentally, as it needs a finite momentum . Theoretically, HB$\chi$PT predicts $G_P$, up to one loop corrections, [10]

$$G_P(q^2) = \frac{2m_\mu g_{\pi pn} f_\pi}{m_\pi^2 - q^2} - \frac{1}{3} g_A m_\mu M_N r_A^2 \tag{5}$$

This result coincides with the well known Adler-Dothan formula [17].

For a momentum transfer of $q_0^2 = 0.88 m_\mu^2$ (which is the momentum transfer in muon capture process on a proton) this means that $g_P = G_P(q_0^2)/m_\mu = 8.23(20)$. Experimentally, however, the situation is not that clear. The induced-pseudo scalar was measured directly on the proton, using muon capture processes. Recently, the MuCap collaboration [18] has used ordinary muon capture (OMC) on a proton, i.e., $\mu^- + p \to \nu_\mu + n$, to determine $g_P = 7.3 \pm 1.2$, as theoretically predicted, though still with a much larger uncertainty.

However, a measurement accomplished in TRIUMF of the radiative muon capture (RMC) on a proton, i.e., $\mu^- + p \to \nu_\mu + \gamma + n$ has resulted in a completely different value, $g_P^{RMC} = 12.8 \pm 1.1$ [19]. The origin of this discrepancy is still unclear. It is thus called for to measure $g_P$ in a different approach. In Section 6, I give a recent use of OMC on $^3$He to extract this observable, a procedure that results in a value consistent with the theoretical approach, with half the uncertainty of the OMC on a proton.

For more information, I refer the reader to a review on the axial structure of the nucleon [16], and to a review regarding the induced pseudo-scalar [21].

## 3 A modern approach for the calculation of weak interaction with light nuclei

Direct measurements of the weak form factors should be performed in the nucleon level, i.e., reactions of leptons on a single nucleon. As mentioned, in some cases, this is indeed possible and leads to sub-percentage accuracy. However, it was demonstrated that in other cases, when such a direct extraction is less successful, one uses weak reactions with nuclei to extract information about the weak structure of the nucleon.

Extracting the nucleon properties from nuclear reactions demands some extrapolation, which stems from the fact that the matrix element of the currents is affected not only by a single nucleon, but also from correlations between nucleons inside the nuclei, especially in the case of the axial current, since it is not conserved. In the language of many-body physics, the effect would be a change in the single nucleon form factors due to in-medium effects. In the few-body mnemonics, this leads to corrections of the weak current inside the nucleus $\mathcal{J}_\mu$ due to exchange currents, i.e.,

$$\mathcal{J}_\mu^{(a)} = \sum_{i=1}^{A} \mathcal{J}_i^{\mu,a} + \sum_{i<j=1}^{A} \mathcal{J}_{ij}^{\mu,a} + ..., \tag{6}$$

where $\mathcal{J}_i^{\mu,a}$ is the contribution of nucleon $i$ to the current (Eqs 2), $\mathcal{J}_{ij}^{\mu,a}$ is the contribution of exchange currents be-

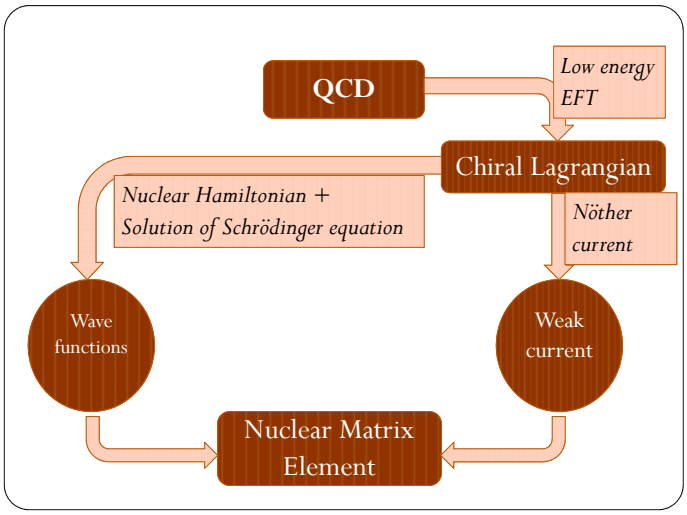


**Fig. 1.** A block diagram of the approach suggested by $\chi$PT to calculate weak reactions.

tween nucleon $i$ and $j$, and the ellipsis stand for correlations between more nucleons. Indeed, it is well established that the theoretical prediction for the half-life of triton, which is an unstable nucleus $\beta$-decaying to $^3$He, overestimates the experimental one, unless one includes many-nucleon contribution to the weak current. However, trying to build the many nucleon currents by using general symmetry arguments, as was done for the nucleon, has two main flaws: (i) it results in too many free parameters, and (ii) in this way one misses any physics behind this current. Moreover, trying to model the currents as meson-exchange currents (MEC) leads to an additional problem in the need to choose the mesonic degrees of freedom that should be taken into account, which leads to model dependent predictions.

Thus main problem in calculating weak reactions with nuclei from the nucleonic degrees of freedom is to systematically add the many-nucleon contributions, which is just reinstating the "holy grail" – to find the matrix element of the currents between nuclear states, directly from QCD. As mentioned, a first principles calculation for this is still out of reach. In the following I briefly outline the modern way to do this, by which one can make use of the symmetries at low energy of QCD and their realizations to give model-independent predictions of dynamical properties. This is done by means of a non-perturbative renormalization group approach to QCD, based on the chiral symmetry of the theory, namely chiral effective field theory ($\chi$PT) (outline and details appear at [22]). One can use the resulting effective $\chi$PT Lagrangian to derive both the nuclear potential, which are the inter-nucleon forces derived from the Lagrangian, as well as the weak currents. Hence, a mutual description of the structure and the scattering process from the same physical origin. This procedure is depicted in Fig. 1.

The $\chi$PT Lagrangian ia constructed by integrating out all degrees of freedom above the merit of the chiral symmetry $\Lambda_\chi \sim 1$ GeV. This dictates that the nucleons and pions are the only explicit degrees of freedom. As such, it retains all conjectured symmetry principles. Of central importance is the approximate chiral symmetry of the underlying theory, originating in the small masses of the up- and down- quarks. Furthermore, each term in the Lagrangian can be characterized by a positive power of $Q/\Lambda_\chi$, where $Q$ is the generic momentum in the nuclear process or the pion mass. This gives a natural organization of the importance of the different terms in the Lagrangian, similar to a perturbative expansion [22]. Though this perturbative expansion has been shown to have some weaknesses [23], mainly in underestimating the order of some terms in the inter-nucleon forces, it is clear that it holds a significant value for the study of the properties of QCD at low energy and its chiral symmetry.

The chiral symmetry dictates the operator structure of each term of the effective Lagrangian, whereas the coupling constants result from the integration out of the higher degrees of freedom. Their value represents information about energies higher than the cutoff of the theory. A theoretical evaluation of these coefficients, or low-energy constants (LECs), is equivalent to solving QCD at low-energy. Recent lattice QCD calculations have allowed a theoretical estimate of LECs of single-nucleon diagrams [24], while LECs of diagrams involving more than one nucleon are out of the reach of current computational resources. Thus, one resorts to constraining these undetermined constants by low-energy experiments.

The chiral expansion is used to derive both nuclear potentials and currents from the same Lagrangian. Therefore, the electroweak dynamics, and the strong interaction dynamics ($\pi N$ scattering, the $NN$ interaction, the $NNN$ interaction, etc.) are all based on the same theoretical grounds and rooted in the low-energy limits of QCD. $\chi$PT predicts the nuclear force and the organization the importance of the different terms: the $NN$ interaction starts at the leading

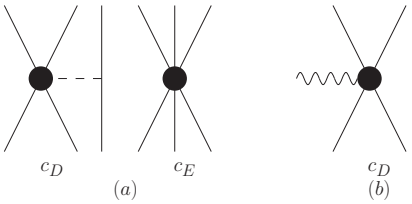


**Fig. 2.** Contact and one-pion exchange plus contact interaction (*a*), and contact MEC (*b*) terms of $\chi$PT. Figure taken from [25].

order (LO), a three-nucleon (*NNN*) interaction at the next-to-next-to-leading order or N$^2$LO [26], and a four-nucleon force at the fourth order (N$^3$LO) [27]. This is the first theoretical verification that the importance of the forces diminishes with the number of nucleons involved. I refer the reader to the contribution of H. Krebs in these proceedings for more information about the forces [28]. The same holds for the current: the LO nuclear current consists of (the standard) single-nucleon terms, while MEC make their first appearance at N$^2$LO [29]. The contribution of T.-S. Park gives a review on these currents [30].

Up to N$^3$LO both the potential and the current are fully constrained by the parameters defining the *NN* interaction, with the exception of two LECs, coined $c_D$ and $c_E$. The latter, $c_E$, appears only in the potential as the strength of the *NNN* contact term [see Fig. 2 (*a*)]. On the other hand, $c_D$ has an effect both in the forces, in the contact term part of the *NN*-$\pi$-*N* three-nucleon interaction of Fig. 2 (*a*) and in exchange currents, in the two-nucleon contact vertex with an external probe of the exchange currents [see Fig. 2 (*b*)].

Thus, fixing these LECs gives a mutual constrain for both phenomena, and allows consistent calculations of weak reactions within $\chi$PT. It should be noticed that MEC involve two nucleons. As a result, one can use a two-nucleon weak process to fix $c_D$, which appears in the forces only in the three nucleon diagrams. Thus,

*a three nucleon force parameter can be calibrated at the two body level (!).*

A most promising reaction to do this is the OMC on the deutron. The problem is that this rate is measured only to 5% accuracy, though a new experiment in PSI, the MuSun experiment, aims to improve this to 1% accuracy. Until this would be fulfilled, a better test ground for such reaction is the triton $\beta$-decay rate, which is very well measured.

In the next sections I give an application of this approach to a few processes, namely triton and $^6$He $\beta$ decays and OMC on $^3$He. These examples are intended to show the validity of the prescribed method. However, the most important contribution is to understand the in-medium structure of the nucleon, as predicted by $\chi$PT. In particular, it gives insight into the axial correlations of nucleons in nuclei, which gives a hint regarding the behavior of the nucleon in heavier nuclei, and an extraction of the vacuum nucleon structure from weak processes in finite nuclei.

## 4 *NNN* force parameters from the consistency of interactions and currents in $\chi$PT [25]

In this section I present a recent calculation which applies the prescription outlined in the previous section for the problem of determining $c_D$ and $c_E$. First attempts to do so have used the triton binding energy (b.e.) alongside an additional strong observable, either the *nd* doublet scattering length [31], or the $^4$He b.e. [32]. However, the correlations between strong observables, in these cases the Phillips and Tjon lines respectively, lead to substantial uncertainty in the extrected values of these LECs. In addition, the fine-tuning of these observables is very sensitive to the structure of the adopted *NNN* force. They are hence sensitive to the details of the $\chi$PT application, such as the specific cutoff, regularization scheme, missing terms of the interaction, etc. In Ref. [33] the two LECs were obtained by complementing the constraint on the $A = 3$ b.e. with a sensitivity study on the radius of $^4$He and on various properties of *p*-shell nuclei. The same interaction was then successfully used to predict the $^4$He total photo-absorption cross section [34].

Thus, an alternative determination of these LECs is needed, due to two main arguments. First, it would be desirable to perform such a determination within the minimal systems possible, $A \leq 3$ systems, as it will suppress any additional many body contribution, and will simplify the calculations. Second, the *NNN* potential has been fully worked out only up to N$^2$LO, leaving inconsistency in the calculation of the wave functions when combined with the NN force at N$^3$LO. Clearly, it would be preferable to adopt an observable with minimal dependence on the short-range part of the wave function. In this respect, the relation between electroweak processes and *NNN*-force effects offers venues to achieve these goals. In particular, Gårdestig and Phillips [35], suggested the triton beta-decay as one of the electroweak processes that could be used as input to fix the strength of the *NNN* force. The study presented in this section accomplished this task and constrained the two undetermined LECs within the three-nucleon sector, in a robust way, that in addition predicts, without any free parameters, various $A = 3$, and 4 properties.

### 4.1 Theoretical formalism for calculating $\beta$ decay processes

A brief reminder of $\beta$-decay process is in place, as well as the formalism used in the calculation. The decay is a weak process, in which an unstable nucleus of charge $Z$ emits an electron and anti-electron-neutrino, leaving a nucleus of charge $Z + 1$. In the current regime this interaction is local, as described in Sec. 2. The decay rate can be calculated using Fermi's Golden rule, and it is proportional to the squared matrix element of the weak Hamiltonian. In all decays treated in this contribution, we discuss either a triton decay, or $^6$He decay, hence the transitions are constrained by a selection rule on the angular-momentum

change in the transition: $\Delta J = 0, 1$. Thus, a multipole decomposition of the nuclear current is helpful. Due to the small momentum-transfer only the $J = 1$ electric multipole of axial-vector symmetry $E_1^A$, and (in the case of triton) also the $J = 0$ coulomb multipole of polar-vector symmetry $C_0^V$ contribute. The leading order contribution to the $E_1^A$ and $C_0^V$ operators are proportional to the Gamow-Teller and Fermi operators, respectively. Thus, it is customary, when discussing the experimental rates, to talk about the empirical Fermi and Gamow-Teller matrix elements, instead of $E_1^A$ and $C_0^V$, using the relations

$$\mathrm{F} \equiv \sqrt{\frac{4\pi}{2J_i+1}}\langle \mathrm{C_0^V} \rangle \,, \tag{7}$$

and

$$\mathrm{GT} \equiv \sqrt{\frac{6\pi}{2J_i+1}}\frac{\langle \mathrm{E_1^A} \rangle}{\mathrm{g_A}} \,. \tag{8}$$

Here, $\langle C_0^V \rangle \equiv \langle f || C_0^V || i \rangle$, and similarly for $\langle E_1^A \rangle$. $J_i$ is the total angular momentum of the initial nucleus.

As discussed by Simpson [36], and later revisited by Schiavilla *et al*. [37,38], the "comparative" half-life is related to the "empirical" GT and F operators thorough

$$(fT_{1/2})_t = \frac{K/(G^2|V_{ud}|^2)}{|\mathrm{F}|^2 + \frac{f_A}{f_V} g_A^2 |\mathrm{GT}|^2} \,. \tag{9}$$

Here, $K = 2\pi^3 \ln 2/m_e^5$ (such that $K/(G^2|V_{ud}|^2) = 6146.6 \pm 0.6$ sec), and $f_A/f_V = 1.00529$ [37] accounts for the small difference in the radiative corrections between vector and axial-vector transitions. For $^6$He, the comparative half-life $(fT_{1/2})_t = 812.8 \pm 3.7$sec [38], thus one extracts $|\mathrm{GT}(^6\mathrm{He})|_{\mathrm{expt}} = 2.161 \pm 0.005$. For triton, $(fT_{1/2})_t = 1129.6 \pm 3$sec [39], thus $|\mathrm{GT}(^3\mathrm{H})|_{\mathrm{expt}} = 1.6560 \pm 0.0026$ [1].

Following Fig. 1, in order to complete a calculation, we have to specify the detailed structure of the weak-current, and to calculate the nuclear wave functions. These will combine to produce the theoretical $E_1^A$, which will be compared to the experimental ones above.

### 4.2 $\chi$PT weak axial currents in the nucleus

As the chiral symmetry is a gauging of the electro-weak interaction, the weak currents are the Nöther currents of this symmetry. Since the momentum transfer is small, the vector current is fully determined by CVC and can be calculated using the Siegert theorem.

The weak axial current adopted here is the Nöther current derived from the axial symmetry of the chiral Lagrangian up to N$^3$LO [29].

At leading order (LO) this current consists of the standard single-nucleon part, which at low momentum transfer is proportional to the Gamow-Teller (GT) operator,

$$E_1^A|_{\mathrm{LO}} = \frac{i\, g_A}{\sqrt{6\pi}} \sum_{i=1}^{A} \sigma_i \tau_i^+ \,, \tag{10}$$

[1] For triton $|\langle C_0^V \rangle| = 0.99955(15)/4\pi$ [38,40].

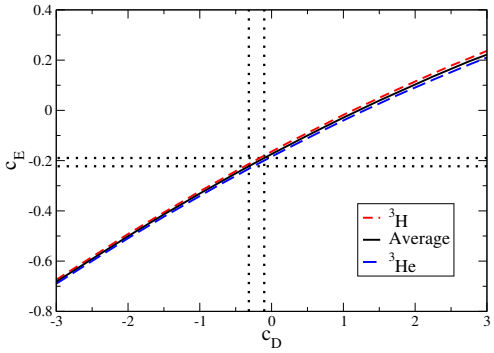


**Fig. 3.** (Color online.) $c_D$-$c_E$ trajectories fitted to reproduce $^3$H and $^3$He experimental b.e. The dotted lines show the region for which $|1 - \langle E_1^A \rangle_{th} / \langle E_1^A \rangle_{emp}|$ is within the ±0.54% error-bars. Figure taken from [25]

where $\sigma_i$, $\tau_i^+$ are spin and isospin-raising operators of the $i$th nucleon.

Corrections to the single-nucleon current appear at the third order of the chiral expansion in the form of relativistic terms. It is easily verified [29] that the single nucleon current achieved in the $\chi$PT formalism, is identical to that achieved in the standard nuclear physics approach (SNPA).

Additional corrections appear in the form of axial MEC. While the relativistic corrections are negligible for the half life, the MEC have a substantial influence on this $\beta$-decay rate. This is a reflection of the fact that $E_1^A$ is a chirally unprotected operator [41]. The MEC, to this order, include two topologies: a one-(charged)-pion exchange, and a contact term (that represents, for example, two-pion exchange or the exchange of heavier mesons) appearing in Fig. 2(b).

Moreover, the LEC determining the strength of the MEC contact term, usually denoted by $\hat{d}_R$, is related to $c_D$ through:

$$\hat{d}_R \equiv \frac{M_N}{\Lambda_\chi g_A} c_D + \frac{1}{3} M_N (c_3 + 2c_4) + \frac{1}{6}. \tag{11}$$

Here, $c_3$ and $c_4$ are LECs of the dimension-two $\pi N$ Lagrangian, already part of the chiral $NN$ potential at NLO. This relation shows that one can use $\langle E_1^A \rangle|_{emp}$ as second constraint for the determination of $c_D$ and $c_E$.

### 4.3 Nuclear wave functions

The nuclear wave functions were calculated in this section in the framework of the no-core shell model (NCSM) approach [32,33,42,2]. This method looks for the eigenvectors of the Hamiltonian in the form of expansions over a complete set of harmonic oscillator (HO) basis states up to a maximum excitation of $N_{\max}\hbar\Omega$ above the minimum energy configuration, where $\Omega$ is the HO parameter.

Thanks to the large model-space size adopted ($N_{\max} = 40$), $A = 3$ b.e. and reduced matrix element of $E_1^A$ are converged to less than 0.05%.

For consistency, the same regulator $F_\Lambda(q^2) = \exp(-q^4/\Lambda^4)$ is used for both $NNN$ terms of the interaction and MEC, a process resulting in a local chiral $NNN$ force

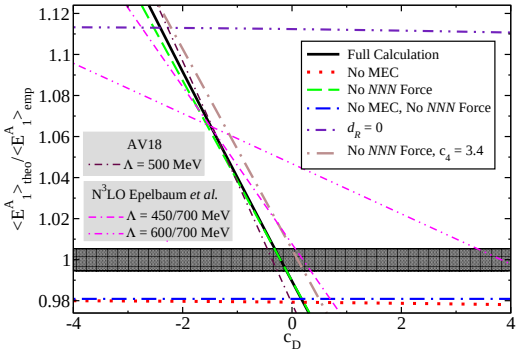


**Fig. 4.** The ratio $\left\langle E_1^A \right\rangle_{th} / \left\langle E_1^A \right\rangle_{emp}$ using the N$^3$LO *NN* potential [44] with and without the local N$^2$LO *NNN* interaction [42], and the axial current with and without MEC ($c_D, c_E$ are varied along the averaged trajectory of Fig. 3). The shaded area is twice the experimental uncertainty. Also shown: results for the phenomenological AV18 potential (with $\Lambda = 500$ MeV imposed in the current), and for the N$^3$LO *NN* potential of Epelbaum et al. [46] (with $\Lambda = 450, 600$ MeV, and a 700 MeV spectral-function cutoff in the two-pion exchange). Figure taken from [25].

(for relevant parameters and definitions see Ref. [42]). The $A = 3, 4$ calculations of Ref. [42] were later confirmed by the results of Ref. [43], providing a benchmark for the local chiral *NNN* force.

In order to choose the possible wave functions, at the first step one builds a $c_D$-$c_E$ trajectory which reproduces, on average, the $A = 3$ b.e.. This curve, appearing in Fig. 3, is taken from Ref [33].

### 4.4 Results and discussion

The calculation steps are as follows: (i) calculate the $^3$H and $^3$He g.s. wave functions by solving the Schrödinger equation for three nucleons interacting via the $\chi$PT *NN* potential at N$^3$LO of Ref. [44] and the *NNN* interaction at N$^2$LO [26] in the local form of Refs. [33,34,42]; (ii) determine for which $c_D$ values along the trajectory the calculated reduced matrix element of the $E_1^A$ operator (at N$^3$LO) reproduces $\left\langle E_1^A \right\rangle_{emp}$.

The ratio of theoretical to empirical value for the $E_1^A$ reduced matrix element along the averaged constraint of Fig. 3 (which reproduces the $A = 3$ b.e. to about 10 KeV [33]) is presented in Fig. 4. The tolerance band highlighted by the shaded area is obtained by doubling the error bar. The uncertainty is determined by uncertainties on $\left\langle E_1^A \right\rangle|_{emp}$ and $g_A$. The full calculation appears as a solid line and shows a strong dependence on $c_D$, indicating a stringent constrain on this parameter.

To this important conclusion, one can add the results of few additional tests, appearing in Fig. 4, that are aimed to probe the axial correlations in the nucleus, by analyzing the sensitivity of the triton half life to *NNN* force and/or MEC:

- *The fundamental importance of the axial two-body currents*. By suppressing the MEC, in the whole investigated $c_D$-$c_E$ range, the calculations under-predict $\left\langle E_1^A \right\rangle|_{emp}$ by about 2%. When adding the the long-range one-pion-exchange term of the MEC, which corresponds to setting $\hat{d}_R = 0$, one gets the same, almost constant behavior. In this case, however, the theoretical results over-predict $\langle E_1^A \rangle|_{emp}$ by ∼11%. Adding the contact part of the MEC, which is related to the short range weak correlations of axial character, cures this problem and allows the half-life to reach its experimental value for $-0.3 \le c_D \le -0.1$. The corresponding $c_E$ values lie in the range $[-0.220, -0.189]$. These results are summarized by the dotted lines in Fig. 3.
- *The negligible effect of the NNN force on this observable* In a similar spirit, a study of the suppression of the *NNN* force is helpful. An attempt to calibrate $c_D$ to reproduce the measured half-life without *NNN* force, results in a curve in close agreement with the results of the full calculation. It is therefore clear that the half life of triton presents a very weak sensitivity to the *NNN* force, and hence to the strength of the spin-orbit interaction.
- *Weak dependence on the specific character of the force* Complementary to the previous point, a quantitatively similar $c_D$ dependence of $\left\langle E_1^A \right\rangle$ can be obtained using $A = 3$ wave-functions produced by the phenomenological AV18 *NN* potential. Fig. 4 shows two additional curves obtained using the N$^3$LO *NN* potential of Ref. [46] with $\Lambda = 450$ and 600 MeV (700 MeV two-pion exchange spectral-function cutoff) and the parameters defining it (particularly, in GeV$^{-1}$, $c_3 = -3.4$ and $c_4 = 3.4$). As one could expect, the extracted value of the *NNN* LEC $c_D$ depends on the choice of the cutoff. However, one observes that the $\Lambda = 450/700$ MeV potential gives comparable results as the N$^3$LO potential of Ref. [44] and AV18, indicating that the determination of $c_D$ depends mainly on the MEC cutoff and weakly on the cutoff imposed in the nuclear potential.

These features, which might be unique to *s*-shell nuclei, entail that the determination of $c_D$ and $c_E$ obtained in this work is robust.

With this calibration of $c_D$ and $c_E$, for this potential, in principle, any other calculation is a prediction of $\chi$PT. In Table 1 a collection of $A = 3$ and 4 data is given, obtained with and without inclusion of the *NNN* force for $c_D = -0.2$ ($c_E = -0.205$)The $NN + NNN$ results for the $^4$He are in good agreement with measurement. Note that $\alpha$ particle g.s. energy and point-proton radii change minimally with respect to variations of $c_D$ in the interval $[-0.3, -0.1]$, and the results at the extremes are both within the numerical uncertainties quoted in Table 1.

Summarizing, using the $A = 3$ b.e. and the half-life of triton it is feasible to constrain the undetermined N$^3$LO $\chi$PT parameter, in a robust way. The constraint on $c_D$ has weak sensitivity with respect to the *NNN* force. The $c_E$ parameter is expected to change due to N$^3$LO terms of the *NNN* interaction, which were not included. This work gives a clear path towards determining the *NNN* force that, once the *NN* interaction will be pinned down, will pave the

**Table 1.** Calculated $^3$H, $^3$He and $^4$He g.s. energies (in MeV) and point-proton radii (in fm), obtained using the N$^3$LO *NN* potential [44] with and without the local N$^2$LO *NNN* interaction [42] with $c_D = -0.2$ and $c_E = -0.205$, compared to experiment.

| | $^3$H | | $^3$He | | $^4$He | |
|---|---|---|---|---|---|---|
| | $E_{\text{g.s.}}$ | $\langle r_p^2\rangle^{1/2}$ | $E_{\text{g.s.}}$ | $\langle r_p^2\rangle^{1/2}$ | $E_{\text{g.s.}}$ | $\langle r_p^2\rangle^{1/2}$ |
| *NN* | −7.852(4) | 1.651(5) | −7.124(4) | 1.847(5) | −25.39(1) | 1.515(2) |
| *NN+NNN* | −8.473(4) | 1.605(5) | −7.727(4) | 1.786(5) | −28.50(2) | 1.461(2) |
| Expt. | −8.482 | 1.60 | −7.718 | 1.77 | −28.296 | 1.467(13) [45] |

way to parameter-free predictions of QCD in the consistent approach provided by $\chi$PT.

## 5 $^6$He $\beta$-decay and the in-medium behavior of the axial constant[47]

Incidentally, the weak dependence of the half life of triton upon the *NNN* force, as found in the previous section, can be used to give some insight into the success of recent calculations done in a hybrid approach, coined EFT* [29].

In EFT*, one uses a nuclear force of phenomenological origin, instead of a $\chi$PT based force, alongside with $\chi$PT based currents. This approach is helpful and pragmatic to bypass problems in applying the $\chi$PT force, as it is not fully published yet.

In this section we make use of EFT* to investigate a different aspect of the weak structure of the nucleon, namely the evolution of the axial constant inside medium.

$\beta$-decay is a process that is rather easy to measure and happens in many nuclei. As such, it provides an experimental window to the properties of a nucleon in a medium of nuclear density.

In particular, theoretical studies of $\beta$-decay rates using shell model calculations, have argued for a suppression of the axial coupling constant $g_A$, from its vacuum value, as extracted from the lifetime of the neutron $g_A = 1.2695 \pm 0.0029$ [14], to unity, i.e. $g_A = 1$ [48,49]. This suppression occurs gradually, as the mass of the nucleus grows, and fully utilized for $A \approx 40$, according to the most recent study [50].

The ramifications of this suppression are numerous. For example, to the understanding of astrophysical phenomena, such as neutron-star cooling and core collapse supernovae, whose dynamics is controlled by the weak interactions. It is of no surprise that the source of this suppression has been the target of many theoretical works, which have associated it with exotic phenomena such as partial restoration of chiral symmetry in finite densities, or less-exotic such as deficiencies in the inclusion of correlations between nucleons, loop-corrections to the axial current originating in nucleonic excitations and mesonic currents, or combination of the three [51–53,55].

These suppression mechanisms assume (or entail) that a full calculation of the weak interaction inside nuclei would bring the theoretical decay-rates to agree with the experimental ones. That is, if one follows the prescription outlined in Fig. 1, then one should recover the physical value of the axial constant. Checking this assumption is possible today only at light nuclei.

The lightest nucleus that undergoes a $\beta$-decay is the triton. However, the theory cannot be checked in the triton since its half-life is used to calibrate the strength of the MEC. The lightest nucleus that can provide a test to the theory is thus $^6$He. Note that this is already a six-body problem, which even in the current computational powers is a challenge. $^6$He ($J^\pi = 0^+$) is an unstable nucleus, which undergoes a $\beta$ decay with a half-life $\tau_{1/2} = 806.7 \pm 1.5$ msec to the ground state of $^6$Li ($J^\pi = 1^+$) [56].

However, a microscopic calculation of $^6$He from its nucleonic degrees of freedom, failed to reproduce the $\beta$-decay rate. This study, accomplished by Schiavilla and Wiringa [38], has used the realistic Argonne $v18$ (AV18) nucleon-nucleon potential, combined with the Urbana-IX (UIX) three-nucleon-force (3NF), to derive the nuclear wave functions, through the variational Monte-Carlo approach. The model used for the nuclear weak axial current includes one- and two-body operators. The two-body currents are phenomenological, with the strength of the leading two-body term – associated with $\Delta$-isobar excitation of the nucleon – adjusted to reproduce the Gamow-Teller matrix element in tritium $\beta$-decay. The calculated half-life of $^6$He overpredicts the measured one by about 9%. An unexpected result of the calculation, was that two-body currents lead to a 1.7% increase in the value of the Gamow-Teller matrix element of $^6$He, thus worsening the comparison with experiment.

Pervin *et* al. [57], have used the GFMC approach to evolve the VMC wave functions ansatz, a process that converges to an exact solution of the quantum problem. Indeed, this brings the single nucleon Gamow-Teller matrix element to about 0-3% deviation from the experimental value. However, the MEC are still expected to increase the deviation from the experiment to about 2-5% from the experimental value, leaving this problem intact.

Here I bring a recent study that argues that the origin of the discrepancy is in the model of the weak interaction inside the nucleus.

The theoretical formalism follows Subsec. 4.1, and the current was presented in Subsec. 4.2. The experimental triton half-life is used to determine the contact LEC $\hat{d}_r$ in Sec. 5.2.1.

The six-body nuclear problem is solved in a fully *ab-initio* approach, expanded in hyperspherical-harmonics function, from its nucleonic degrees of freedom [58–60]. The nuclear wave functions are derived from J-matrix in-

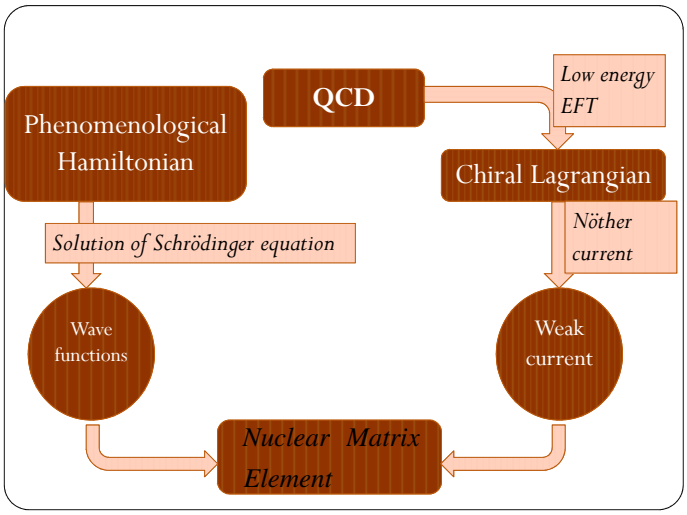


**Fig. 5.** A block diagram of the approach suggested by EFT* to calculate weak reactions

verse scattering nucleon-nucleon potential (JISP), describing two-nucleon scattering data and bound and resonant states of light nuclei to high accuracy

### 5.1 Nuclear Wave Functions

The difference between the one-body contribution to the $^6$He-$^6$Li GT matrix element and the experimental value is of the order of few percent, thus the needed numerical accuracy has to be at a *per mil* level. In view of this required level of convergence we use the JISP16 potential [61–63], to model the interaction between the nucleons. The JISP16 NN potential utilizes the J-matrix inverse scattering technique to construct a soft nuclear potential, formulated in the harmonic oscillator basis, that by construction reproduces the NN phase shifts up to pion threshold and the binding energies of the light nuclei with $A \leq 4$. For recent advances, see A. Shirokov's contribution [64].

We use the Hyperspherical-Harmonics (HH) expansion to solve the Schrödinger equation. The HH functions constitute a general basis for expanding the wave functions of an $A$-body system [66]. They constitute a complete set of antisymmetric basis functions in the Hilbert space of spin, isospin and hyperangles. The functions are characterized by a set of quantum numbers $[K]$ [59,60] and possess definite angular momentum, isospin, and parity quantum numbers. They are the eigenfunctions of the hyperspherical, or generalized angular momentum operator $\hat{K}^2$, $\hat{K}^2 \mathcal{Y}_{[K]}(\Omega, s_i, t_i) = K(K+3A-5)\mathcal{Y}_{[K]}(\Omega, s_i, t_i)$. The expansion is characterized by $K$, the (grand angular momentum) quantum number of $\hat{K}$. The details of this method are explained thoroughly in Ref. [65].

### 5.2 Results

#### 5.2.1 The triton $\beta$-decay - Calibration of $\hat{d}_r$

The results for the ground state properties of the $A = 3$ nuclei, $^3$H and $^3$He, are presented in table 2. The results are variational.

**Table 2.** The JISP16 NN interaction $^3$He, $^3$H binding energies, rms matter radius, and the leading order GT matrix element as a function of $K_{max}$.

| | $^3$H | | $^3$He | | |
|---|---|---|---|---|---|
| $K_{max}$ | B.E. | radius | B.E. | radius | $GT\|_{LO}$ |
| 4 | 8.094 | 1.632 | 7.364 | 1.653 | 1.6656 |
| 6 | 8.233 | 1.656 | 7.512 | 1.680 | 1.6620 |
| 8 | 8.319 | 1.677 | 7.604 | 1.704 | 1.6575 |
| 10 | 8.351 | 1.691 | 7.641 | 1.720 | 1.6547 |
| 12 | 8.360 | 1.697 | 7.651 | 1.727 | 1.6538 |
| 14 | 8.365 | 1.701 | 7.657 | 1.733 | 1.6530 |
| 16 | 8.367 | 1.704 | 7.660 | 1.736 | 1.6526 |
| 18 | 8.367 | 1.705 | 7.661 | 1.738 | 1.6524 |
| $[63]_V$ | 8.354 | | 7.648 | | |
| $[63]_E$ | 8.496(20) | | 7.797(17) | | |
| Exp. | 8.482 | | 7.718 | | |

The results indicate that the JISP16 potential leads to an underbinding of about 80keV for the $^3$He and 120keV for the triton, and are in good agreement with the variational NCSM results of Shirokov *et* al. [63], though a discrepancy of about 130keV exists with their effective interaction results $[63]_E$.

Comparing the JISP16 leading order GT matrix element with those of other potential models, see table 3, one

observes that the JISP16 potential model leads to an enhancement of the 1-body matrix element and it almost coincides with the experimental value.

**Table 3.** The dependence of the triton $\beta$-decay leading order GT matrix-element on the potential model.

| Potential model | $GT\|_{LO}$ |
|---|---|
| AV18+3NF [67] | 1.598(2) |
| Bonn+3NF [68] | 1.621(2) |
| Nijm+3NF [69] | 1.605(2) |
| $N^3LO$+3NF [25] | 1.622(2) |
| UCOM [73] | 1.65(1) |
| JISP16 [47] | 1.6524(2) |
| Expt. | 1.656(3) |

Now it is possible to use these wave functions to determine the LEC $\hat{d}_r$, by calibrating the MEC to give the additional strength needed to fit the experimental value. The following calibration for $\hat{d}_r(\Lambda_\chi)$ is achieved:

$$\begin{aligned}\hat{d}_r(\Lambda_\chi = 500\,\mathrm{MeV}) &= 0.583(27)_t(38)_{g_A}\\ \hat{d}_r(\Lambda_\chi = 600\,\mathrm{MeV}) &= 0.625(25)_t(35)_{g_A}\\ \hat{d}_r(\Lambda_\chi = 800\,\mathrm{MeV}) &= 0.673(23)_t(33)_{g_A}.\end{aligned} \tag{12}$$

The numbers in parenthesis denote uncertainties in the last digits. The first error is due to the uncertainty in the triton half-life, whereas the second one is due to uncertainty in $g_A$ (the numerical error is negligible).

#### 5.2.2 The $^6$He-$^6$Li Gamow-Teller matrix-element

Turning now to the $A = 6$ case, table 4 presents the ground state properties of the $^6$He, and $^6$Li nuclei. Evidently, at the value $K_{max} = 14$, which corresponds to about $2 - 3 \cdot 10^6$ basis states, the binding energies of the 6-body nuclei are calculated with an accuracy of few hundreds keV.

One can extrapolate the results for the binding energies, to get 28.70MeV for $^6$He and 31.46MeV for $^6$Li. These results underestimate the experimental energies by about 0.5 MeV, though the difference $\Delta E = 2.76$MeV differs by merely 34keV from the experimental value.

The leading order value for the GT, calculated using the JISP16 potential, is in accordance with the values GT = 2.28 for AV8'/TM'(99) and GT = 2.30 for AV8' [70], GT = 2.28 for the $N^3LO$ NN-force [71], GT = 2.25 for AV18/UIX [38], and GT = 2.16 – 2.21 for AV18/IL2 [57]. Moreover, the accuracy in estimating the GT matrix element is at the level of *per mil*, enabling a research of the axial MEC model.

Incorporating the $\chi$PT based contributions to the weak-current one can calculate the full $^6$He-$^6$Li GT matrix-element at the $N^3LO$ level, as a function of the cutoff imposed in the weak current:

$$|\mathrm{GT}(^6\mathrm{He})|_{\mathrm{theo}} = 2.198(1)_\Lambda(2)_N(4)_t(5)_{g_A} = 2.198 \pm 0.007 \tag{13}$$

The first error is the cutoff variation dependence, the second is numerical, the third is due to uncertainties in the triton half-life, and the last is due to uncertainties in $g_A$. This should be compared to the experimental matrix-element $|\mathrm{GT}(^6\mathrm{He})|_{\mathrm{expt}} = 2.161 \pm 0.005$. Thus, the theory overpredicts GT by about 1.7%.

### 5.3 Discussion

The use of phenomenologically based potential, JISP, combined with a $\chi$PT based MEC, is an inconsistency inherent to this calculation. Clearly, a more consistent calculation, in the form presented in Sec. 4 is called for. This inconsistency, however, allows to accomplish the task of a microscopic calculation of a six-body problem.

It is hard to estimate the effect of the approximation in this inconsistency, but according to Sec. 4 we expect a weak dependence of the GT value on the specific character of the force. In addition, the JISP potential successfully reproduces nucleon-nucleon scattering data, and the binding energies of $A < 16$ mass nuclei. The minimal dependence of the half-life in the cutoff gives additional reassurance.

One concludes that the qualitative difference originates in the different structure of the SNPA and $\chi$PT based MEC. A careful analysis of the difference between the MEC originating in $\chi$PT and those used in SNPA, has been accomplished by Park *et al* [29]. They have shown that one-pion exchange term exists in both models. Of particular importance is the part of this term in the SNPA based MEC that represents the exchange of a pion due to a delta excitation of the nucleon, which is found to correspond roughly to the $\hat{c}_3$ term in the $\chi$PT based MEC. The coupling constant of this term $g_{\pi N\Delta}$ has been fixed by Schiavilla and Wiringa [38], so that the theory would reproduce the triton half-life.

However, differences between the approaches arise in their short range character. In the SNPA approach, these correspond to the exchange of a $\rho$-meson. Such a term does not exist in the $\chi$PT approach as it arises only at $N^5LO$ [29]. Moreover, a contact interaction does not appear in the SNPA approach. It is this contact interaction that creates the qualitative difference between the current work and that of Schiavilla and Wiringa [38].

In order to acknowledge that, Fig. 8 gives the relative contribution of each the terms, i.e. one-body, one-pion-exchange and full calculation, to the GT matrix element. One first recognizes that the one-pion contribution to the matrix element has a positive sign in both $^3$H and $^6$He, and that the contact interaction has a negative contribution to the matrix element. In the case of $^3$H this is only a partial cancelation, as it is calibrated to increase the 1-body matrix element and to bring the calculation into the experimental value. It is important to notice that the same partial cancelation is found also in the calculation of Sec. 4, indicating that it is not a result of the use of the JISP potential.

In contrast to $^3$H, when examining the case of $^6$He, one observes that the negative contribution of the contact term is bigger (in absolute value) than the one-pion-exchange contribution, thus leading to a total negative contribution

**Table 4.** The JISP16 NN interaction $^6$He, $^6$Li binding energies, rms matter radii, and the leading order GT matrix element as a function of $K_{max}$.

| | $^6$He | | $^6$Li | | |
|---|---|---|---|---|---|
| $K_{max}$ | B.E. | radius | B.E. | radius | $GT\|_{LO}$ |
| 4 | 18.367 | 1.840 | 19.392 | 1.859 | 2.263 |
| 6 | 24.103 | 1.902 | 26.124 | 1.909 | 2.247 |
| 8 | 26.392 | 1.979 | 28.854 | 1.984 | 2.234 |
| 10 | 27.560 | 2.051 | 30.156 | 2.051 | 2.232 |
| 12 | 28.112 | 2.112 | 30.797 | 2.110 | 2.229 |
| 14 | 28.424 | 2.165 | 31.132 | 2.160 | 2.227 |
| ∞ | 28.70(13) | | 31.46(5) | | 2.225(2) |
| [63] | 28.32(28) | | 31.00(31) | | |
| Exp. | 29.269 | 2.18 | 31.995 | 2.09 | 2.170 |

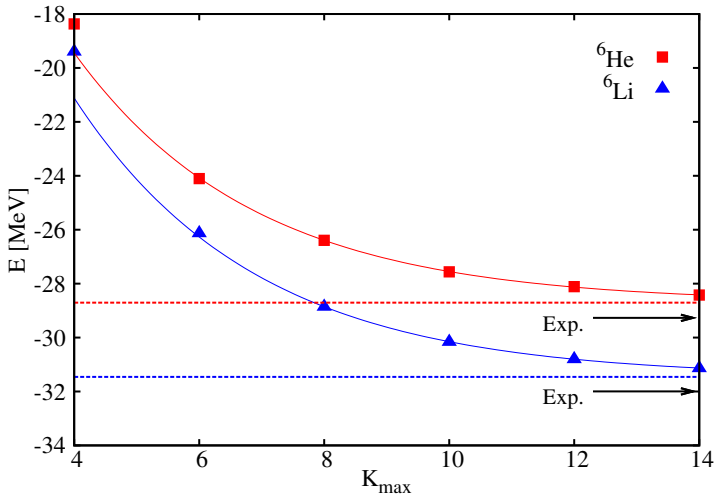


**Fig. 6.** The convergence of the binding energies of the 6-body nuclei, $^6$Li and $^6$He. The continuous lines are the fits $E(K_{max}) = E_\infty + Ae^{-\alpha K_{max}}$. The dashed lines are the extrapolated values $E_\infty$. The experimental values are marked with black arrows. Figure taken from [47].

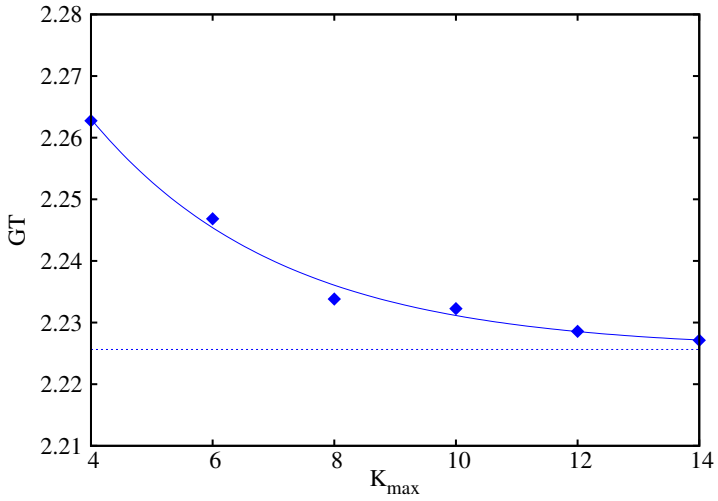


**Fig. 7.** The convergence of the GT matrix element for the $^6$He-$^6$Li $\beta$-decay. The continuous line is the fit $GT(K_{max}) = GT_\infty + Be^{-\beta K_{max}}$, the dashed line is the extrapolated value $GT_\infty$. Figure taken from [47].

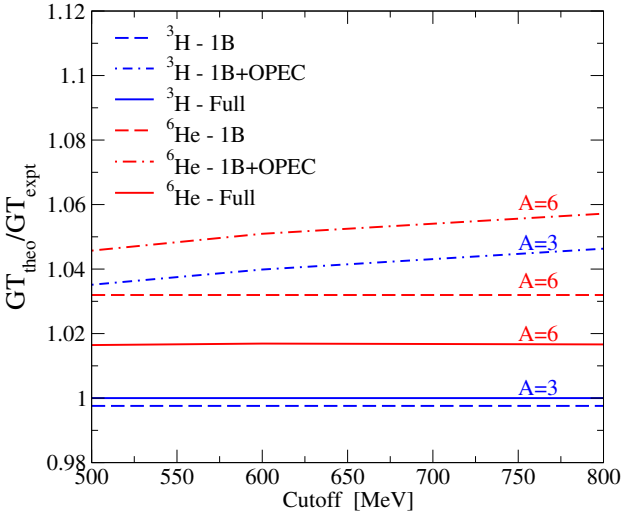


**Fig. 8.** Relative contributions to the theoretical GT matrix elements as a function of the EFT cutoff. All the results are normalized to the empirical values. The blue lines indicated by $A = 3$ correspond to the $^3$H-$^3$He $\beta$-decay. The red lines indicated by $A = 6$ correspond to the $^6$He-$^6$Li case. Dashed lines correspond to the 1-body impulse approximation (1B). Dashed-dotted lines correspond to 1-body plus one-pion exchange current (OPEC). Continuous lines correspond to full calculation (note that in the case of $^3$H this is calibrated to give exactly the experimental value). Figure taken from [47].

of the MEC. This negative contribution is needed as the single-nucleon GT is bigger than the experimental GT.

Recalling the fact that the SNPA approach does not contain a contact interaction, we understand the origin of the positive contribution of the MEC in that approach, which increases the difference between the calculated and measured decay-rates.

The agreement between the calculated and measured decay rates of $^6$He indicates that there is no signature in this observable for an additional suppression of the axial constant. It appears that all the needed suppression originates in correlations between nucleons in the nucleus, revealing itself in the form of exchange currents.

## 6 Extracting the weak structure of the nucleon from $\mu^-$ capture on $^3$He [72]

In this section, I use the $\mu^-$ capture process on $^3$He that results in $^3$H, to extract the weak structure of the nucleon.

This sizable momentum transfer in OMC processes enhances the effect of the induced-pseudoscalar form factor, thus allowing its study.The MuCap measurement of OMC on a proton [18] has already reached a ±2.4% determination of the capture rate, and aims to ±1%. This leads to the tightest experimental bound on the induced-pseudo scalar form factor of the nucleon, constraining its value to ±15% [18]. In addition, one can use OMC to study second class currents [8].

Further reduction of the uncertainties in these three form-factors demands sub-percentage experimental accuracy, which is hard to achieve in $\mu^- p$ process, since its rate is smaller than the free muon decay rate by a factor bigger than 500, and since it results in the emission of neutral particles. These obstacles can be removed for heavier nuclei, as the capture rate is very sensitive to the nuclear charge, scaling as $Z^4$. Alas, due to the strong correlation between nucleons, theoretical microscopic studies with sub-percentage precision, are possible only in very light nuclei.

The capture of muon on $^3$He which results in a triton, $\mu^- + ^3\text{He} \rightarrow \nu_\mu + ^3\text{H}$, provides such opportunity. It has an extraordinarily accurate measured capture rate $\Gamma(\mu^- + ^3\text{He} \rightarrow \nu_\mu + ^3\text{H})^{\text{exp}} = 1496(4)\,\text{Hz}$, i.e. a ±0.3% precision [20].

This precision measurement has already induced a number of theoretical works, among them are also microscopic theoretical studies of the reaction [21,74,75]. However, all these studies missed an important, recently discovered, ingredient. Lately [76], the electroweak radiative corrections to the capture process have been calculated. The results indicate that the enhancement factor due to this effect is RC(He) = 0.030(4). In addition, all these works included free parameters in the mesonic currents. In view of previous section, a calculation within EFT or EFT* is called for. I present here the latter: the calculation uses the $\chi$PT weak current combined with the phenomenological nucleon-nucleon potential Argonne $v_{18}$ (AV18) [77] augmented by the Urbana IX (UIX) [78] three nucleon force. This calculation is used to put constraints on the weak form factors of the nucleon, including the second class terms, which was not done previously in microscopic calculations. The calculation is parameter free, thus can be used to make predictions.

### 6.1 Theoretical Formalism

A brief reminder of muon capture process, and the formalism used in the calculation is in place. The muonic atom, a bound state of a muon and a nucleus, is unstable. It has two main possible decay schemes, either through free muon decay to lighter leptons, or through a weak muon capture by the nucleus. The probability for the latter is proportional to the probability of muon to be found inside the nucleus, that scales like $Z^3$, and to the number of protons that can lead to the capture. This leads to the famous $Z^4$ scaling of OMC rates. The deviations from this scaling are due to nuclear correlations, and calculating them is challenging, as explained throughout this paper.

The Golden rule is used to write the capture rate [75]:

$$\Gamma = \frac{2G^2|V_{ud}|^2 E_\nu^2}{2J_{^3\text{He}}+1}\left(1-\frac{E_\nu}{M_{^3\text{H}}}\right)|\psi_{1s}^{av}|^2\Gamma_N, \qquad (14)$$

where $J_{^3\text{He}} = \frac{1}{2}$ is the total angular momentum of the $^3$He. The effects of the nuclear interaction are embedded in the nuclear matrix element $\Gamma_N$, which can be written using

multipole decomposition:

$$\Gamma_N = \sum_{J=0}^{\infty} \left| \left\langle {}^3\mathrm{H} || \hat{C}_J - \hat{L}_J || {}^3\mathrm{He} \right\rangle \right|^2 + \\ + \sum_{J=1}^{\infty} \left| \left\langle {}^3\mathrm{H} || \hat{E}_J - \hat{M}_J || {}^3\mathrm{He} \right\rangle \right|^2 . \quad (15)$$

$\hat{C}_J, \hat{L}_J, \hat{E}_J, \hat{M}_J$ are the Coulomb, longitudinal, transverse electric and transverse magnetic multipole operators of angular momentum $J$, built from the charged nuclear current.

### 6.2 Results

The calculation process demands fixing $\hat{d}_r(\Lambda)$ by reproducing the experimental triton half–life. The resulting cutoff dependence of $\hat{d}_r(\Lambda)$ is:

$$\begin{aligned} \hat{d}_r(\Lambda = 500\,\mathrm{MeV}) &= 1.05(6)_t(0)_N \\ \hat{d}_r(\Lambda = 600\,\mathrm{MeV}) &= 1.82(7)_t(1)_N \\ \hat{d}_r(\Lambda = 800\,\mathrm{MeV}) &= 3.88(9)_t(2)_N \end{aligned} \quad (16)$$

The first error is due to the triton half life, while the second is due to numerics.

The results for the nuclear matrix element of the muon capture process show a 9% effect due to the MEC contribution, and a small effect due to the cutoff dependence of the HB$\chi$PT, within 0.3%. One can average this dependence, and arrive at the prediction: $\Gamma_N = 0.7075(10)$. It is worthwhile noting that the relative contribution of the MEC to this process is almost three times bigger than the MEC contribution to the triton half life. An extremely weak cutoff dependence shows that the essential physics is captured in the HB$\chi$PT operators.

Thus, the final prediction for the capture rate is

$$\Gamma = 1499(2)_\Lambda(3)_{\mathrm{NM}}(5)_t(6)_{\mathrm{RC}}\,\mathrm{Hz}, \quad (17)$$

where the first error is due to the HB$\chi$PT cutoff, the second is due to uncertainties in the extrapolation of the form factors to finite momentum transfer, and in the choice of the specific nuclear model, the third error is related to the uncertainty in the triton half life, and the last error is due to theoretical uncertainty in the electroweak radiative corrections calculated for nuclei [76]. This sums to a total error estimate of about 1%.

As mentioned, the radiative corrections, which are the source of the largest contribution to the error estimation, are not taken into account in previous studies [75,74]. One could reduce the large uncertainty in this contribution, by extending the work in Ref. [76] to include higher order effects and incorporating nuclear effects.

### 6.3 Discussion

The conservative error estimation still allows rather interesting conclusions. First, one notices that the calculated capture rate agrees with the experimental measurement $\Gamma(\mu^- + {}^3\mathrm{He} \to \nu_\mu + {}^3\mathrm{H})^{\mathrm{exp}}_{\mathrm{stat}} = 1496(4)\,\mathrm{Hz}$. Thus, one concludes that EFT* accurately predicts the capture rate.

However, the most interesting result concerns the weak form factors of the nucleon. In order to constrain the induced pseudoscalar and second class form factors, we take the following approach. In each case, we set all the other form factors to their nominal value, and change this form factor in a way which keeps an overlap between the experimental rate and the theoretically allowed rate. The nominal value of the form factor is set to reproduce the experimental measurement.

The resulting constraint on the induced pseudoscalar form factor is:

$$g_P(q^2 = -0.954 m_\mu^2) = 8.13 \pm 0.6\,, \quad (18)$$

in very good agreement with the HB$\chi$PT prediction of Eq. (5). Together with the MuCap results [18], $g_P(q^2 = -0.88 m_\mu^2) = 7.3 \pm 1.2$, this is a great success to the HB$\chi$PT prediction.

A second conclusion concerns the contribution of second class currents. The axial G-parity breaking term was predicted, based on QCD sum-rules to be $\frac{G_t}{g_A} = -0.0152(53)$ [79]. Using this prediction does not change the result of the current calculation significantly (about 0.15%). Our constraint has a much larger error bar than this calculation, and agrees with a vanishing form factor:

$$\frac{G_t}{g_A} = -0.1 \pm 0.68\,. \quad (19)$$

Wilkinson [80] has collected the experimental data to get $|G_t| < 0.3$ at 90% CL, which is a factor of 2 better than the current limit. One has to still consider that the G-parity breaking terms can also excite mesonic currents in the nucleus, which were not taken into account in the current discussion.

This calculation puts the tightest limit on CVC, constraining $m_e F_S / F_V = (0.5 \pm 2) \times 10^{-4}$, which is consistent with CVC. One notes that this is already close to the regime of CVC breaking, predicted by $\chi$PT [10].

## 7 Summary

This review tries to put few-body nuclear physics as a pivot between QCD and the nuclear regime. Few-body calculations of weak reactions can be put, using $\chi$PT, on common grounds with the nucleon. This can be used to extract the properties of the nucleon, and to understand its role inside heavier nuclei.

The future of this field is bright, due to the combination of sub-percentage numerical accuracy in the solution of the quantum problem, alongside with stronger theoretical grounds rooted in QCD, in the form of $\chi$PT. This combination allows parameter free calculations, that can be used in various fields: from constraining the fundamental theory, through understanding nuclear structure, and up to predicting weak reactions for the use of astrophysicists.

## References


1. N. Barnea, W. Leidemann, G. Orlandini, Phys. Rev. **C61** (2000) 054001; N. Barnea, W. Leidemann, G. Orlandini, Nucl. Phys. **A693** (2001) 565;
2. P. Navrátil *et al*., Phys. Rev. Lett. **84** (2000) 5728; Phys. Rev. **C62** (2000) 054311.
3. M. Viviani, A. Kievsky, and S. Rosati, Few-Body Syst. **18** (1995) 25.
4. B.S Pudliner, V. R. Pandharipande, J. Carlson, S. C. Pieper, and R.B. Wiringa, Phys. Rev. **C56** (1997) 1720; Phys. Rev. **C62** (2000) 014001; S.C. Pieper and R.B. Wiringa, Annu. Rev. Nucl. Part. Sci. **51** (2000) 53; S.C. Pieper, K. Varga, and R.B. Wiringa, Phys. Rev. **C66** (2000) 04431.
5. W. Glockle and H. Kamada, Phys. Rev. Lett. **71** (1993) 971; F. Ciesielski and J. Carbonell, Phys. Rev. **C58** (1998) 58;
6. J.S. Real, *Proc. of this Conference*.
7. S. Weinberg, Phys. Rev. **112** (1958) 1375.
8. N. Severijns, M. Beck, and O. Naviliat-Cuncic, Rev. Mod. Phys. **78** (2006) 991.
9. S.S. Gerstein and Ya.B. Zel'dovich, Sov. Phys. JETP **2** (1956) 576; R.P. Feynman and M. Gell Mann, Phys. Rev. **109** (1958) 193.
10. N. Kaiser, Phys. Rev. **C64** (2001) 028201.
11. J.C. Hardy and I.S. Towner, Phys. Rev. **C79** (2009) 055502.
12. G.A. Miller and A. Schwenk, Phys. Rev. **C78** (2008) 035501.
13. E. Caurier, P. Navratil, W. E. Ormand, and J. P. Vary, Phys. Rev. **C66** (2002) 024314.
14. C. Amsler *et al*., Phys. Lett. **B**667, (2008) 1.
15. D. Gazit and H.-U. Yee, Phys. Lett. **B670** (2008) 154.
16. V. Bernard, L. Elouadrhiri, and U.-G. Meissner, J. Phys. G: Nucl. Part. Phys. **28** (2002) R1-R35.
17. S.L. Adler, Y. Dothan, Phys. Rev. **151** (1966) 1267.
18. V.A. Andreev *et al*., Phys. Rev. Lett. **99** (2007) 032002.
19. D.H. Wright, *et al*., Phys. Rev. **C57** (1998) 373.
20. P. Ackerbauer, *et al*., Phys. Lett. **B417** (1998) 224.
21. T. Gorringe, H.W. Fearing, Rev. Mod. Phys. **76** (2003) 31.
22. S. Weinberg, Physica **9**6A (1979) 327; Phys. Lett. **B251** (1990) 288; Nucl. Phys. **B363** (1991) 3; G. Gasser and H. Leutwyler, Ann. Phys. **1**58 (1984) 142.
23. A. Nogga, R.G.E. Timmermans, and U. van-Kolck, Phys. Rev. **C72** (2005) 054006; M. C. Birse, *ibid* **74** (2006) 014003.
24. See, e.g., P. Boucaud *et al.*, Phys. Lett. **B**650 (2007) 304; H.-W. Lin, PoS **L**AT2006 (2006) 185.
25. D. Gazit, S. Quaglioni, and P. Navratil, Phys. Rev. Lett. **103** (2009) 102502.
26. U. van Kolck, Phys. Rev. **C**49 (1994) 2932; E. Epelbaum *et al*., Phys. Rev. **C66** (2002) 064010.
27. E. Epelbaum, Phys. Lett. **B639** (2006) 465.
28. H. Krebs, *Proc. of this Conference*.
29. T.-S. Park, *et al*., Phys. Rev. **C 67** (2003) 055206; M. Rho, nucl-th/0610003; D. Gazit, Ph.D. thesis, Hebrew University, Israel, 2007.
30. T.-S. Park, *Proc. of this Conference*.
31. E. Epelbaum *et al*., Phys. Rev. **C66** (2002) 064001.
32. A. Nogga *et al*., Phys. Rev. **C73** (2006) 064002.
33. P. Navrátil *et al*., Phys. Rev. Lett. **99** (2007) 042501.
34. S. Quaglioni and P. Navrátil, Phys. Lett. **B652** (2007) 370.
35. A. Gårdestig and D.R. Phillips, Phys. Rev. Lett. **96** (2006) 232301.
36. J.J. Simpson, Phys. Rev. **C35** (1987) 752.
37. R. Schiavilla, *et al*., Phys. Rev. **C 58** (1998) 1263.
38. R. Schiavilla and R.B. Wiringa, Phys. Rev. **C 65** (2002) 054302.
39. Yu.A. Akulov and B.A. Mamyrin, Phys. Lett. **B**610 (2005) 45.
40. S. Vaintraub, Master's thesis, The Hebrew University of Jerusalem, Israel (2008).
41. M. Rho, Phys. Rev. Lett. **10** (1991) 1275.
42. P. Navrátil, Few Body Syst. **41** (2007) 117.
43. A. Kievsky *et al*., J. Phys. **G35** (2008) 063101.
44. D. R. Entem and R. Machleidt, Phys. Rev. **C68** (2003) 041001(R).
45. E. Borie and G.A. Rinker, Phys. Rev. **A18** (1978) 324; S. Kopecky *et al*., Phys. Rev. Lett. **74**, (1995) 2447; P. Mohr and B. Taylor, Rev. Mod. Phys. **596** (1996) 367; I. Sick, Phys. Lett. **B576** (2003) 62.
46. E. Epelbaum, W. Glöckle, and U.-G. Meißner, Nucl. Phys. **A747** (2005) 362.
47. S. Vaintraub, N. Barnea, and D. Gazit, Phys. Rev. **C79** (2009) 065501.
48. B. Buck and S. M. Perez, Phys. Rev. Lett. **50** (1982) 1975.
49. D. H. Wilkinson, Nucl. Phys. **A209** (1973) 470.
50. W.-T. Chou, E. K. Warburton, and B. A. Brown, Phys. Rev. **C47** (1993) 163.
51. F. Osterfeld, Rev. Mod. Phys. **64** (1992) 491.
52. M. C. Birse, J. Phys. **G20** (1994) 1537.
53. M. Rho, Phys. Rev. Lett. **54** (1985) 767.
54. E. Caurier, G. Martinez-Pinedo, F. Nowacki, A. Poves, and A. P. Zuker, Rev. Mod. Phys. **77** (2005) 427.
55. W. Weise, Nucl. Phys. **A553**, 59c (1993).
56. F. Ajzenberg-Selove, Nucl. Phys. **A490** (1998) 1.
57. M. Pervin, S. C. Pieper, and R. B. Wiringa, Phys. Rev. **C 76** (2007) 064319.
58. A. Novoselsky and N. Barnea, Phys. Rev. **A51** (1995) 2777.
59. N. Barnea andA.Novoselsky, Ann. Phys. (NY) **256** (1997) 192.
60. N. Barnea and A. Novoselsky, Phys. Rev. **A57** (1998) 48.
61. A. M. Shirokov, A. I.Mazur, S. A. Zaytsev, J. P. Vary, and T. A. Weber, Phys. Rev. **C 70** (2004) 044005.
62. A. M. Shirokov, J. P. Vary, A. I. Mazur, and T. A. Weber, Phys. Lett. **B644** (2007) 33.
63. A. M. Shirokov, J. P. Vary, A. I. Mazur, S. A. Zaytsev, and T. A. Weber, Phys. Lett. **B621** (2005) 96.
64. A. M. Shirokov, *Proc. of this Conference*.
65. N. Barnea, W. Leidemann, and G. Orlandini, Phys. Rev. **C74** (2006) 034003.
66. M. Fabre de la Ripelle, Ann. Phys. (NY) **147** (1983) 281.

67. R.B. Wiringa, V.G.J. Stoks, and R. Schiavilla, Phys. Rev. **C51** (1995) 38.
68. R. Machleidt, Phys. Rev. **C63** (2001) 024001.
69. V.G.J. Stoks, R.A.M. Klomp, C.P.F. Terheggen, and J.J.de Swart, Phys. Rev. **C 49** (1994) 2950.
70. P. Navratil and W.E. Ormand, Phys. Rev. **C 68** (2003) 034305
71. P. Navratil and E. Caurier, Phys. Rev. **C69** (2004) 014311.
72. D. Gazit, Phys. Lett. **B666** (2008) 472.
73. D. Gazit and S. Bacca (unpublished, 2007); S. Bacca, Phys. Rev. **C 75** (2007) 044001.
74. J.G. Congleton, E. Truhlík, Phys. Rev. **C53** (1996) 956.
75. L.E. Marcucci, *et al*., Phys. Rev. **C66** (2002) 054003.
76. A. Czarnecki, W.J. Marciano, A. Sirlin, Phys. Rev. Lett. **99** (2007) 032003.
77. R.B. Wiringa, V.G.J. Stoks, R. Schiavilla, Phys. Rev. **C51** (1995) 38.
78. B.S. Pudliner, et al., Phys. Rev. **C56** (1997) 1720.
79. H. Shiomi, J. Korean Phys. Soc. **29** (1996) S378.
80. D.H. Wilkinson, Eur. Phys. J. A Suppl. **7** (2000) 307